Mechanisms of liquid imbibition in Douglas-fir inferred from 1H Nuclear Magnetic Resonance methods

Dang-Mao Nguyen, Sabine Caré, Denis Courtier-Murias, Meng Zhou, Philippe Coussot

Soumis et accepté à HOLZFORSHUNG (18 Juin 2020)

Short title: **Imbibition in softwood observed by ^{1}H NMR methods**

Mechanisms of liquid imbibition in Douglas-fir inferred from ^{1}H Nuclear Magnetic Resonance methods

Dang Mao NGUYEN [1], Sabine CARE [1,] *, Denis COURTIER-MURIAS [1], Meng ZHOU [1], Philippe COUSSOT [1]

[1] *Lab. Navier, Ecole des Ponts, Univ Gustave Eiffel, CNRS, Marne-la-Vallée, France*

* *sabine.care@univ-eiffel.fr*

Abstract: This study aims at identifying the mechanisms of oil and water imbibition in heartwood and sapwood of Douglas-fir through a combination of original experiments with Magnetic Resonance Imaging (MRI) and Nuclear Magnetic Resonance (NMR) relaxation measurements for oil and free water, and deformation measurements for bound water. Experiments by weighing are performed to verify whether the imbibition process is also consistent with Washburn law. All the results are discussed taking into account the structure of wood (tubular tracheids closed at their tips, but possibly connected to each other via open pits on the side faces) and the preparation of samples.

The observation of relatively fast oil flow imbibition confirms that sapwood exhibits a connected hydraulic network through which a liquid can a priori flow and climb along the structure. However, the spontaneous water imbibition is strongly damped by its very poor wetting when in contact with cell-walls only partially saturated with bound water, so that the diffusion of bound water control the uptake dynamics. However, due to preferentially closed pits, the heartwood does not exhibit a continuous hydraulic network and water essentially penetrates into wood by diffusion through the cell walls.

Keywords: Free and bound water, Magnetic Resonance Imaging, Nuclear Magnetic Resonance Relaxation, oil, permeability, softwood, Washburn.

Introduction

Water transport in wood material plays a major role with regard to its physical properties in various situations, leading to a possible deterioration in performance of the timber elements. Moreover, liquid (oil or water) impregnation to make the wood more resistant to decay or to improve the process of peeling of wood logs for new product design (e.g. Plywood) is an important subject in wood sciences. Therefore, it is crucial to understand how liquid penetrates in the wood material. Liquid transfer in wood materials has been widely studied (Bao et al. 1986, Siau 1995, Elaieb 2014 and 2016, Johansson et al. 2011, Dupleix et al. 2013), it depends on the permeability of wood, the viscosity of liquid as well as its wetting ability (Kučerová 2012, Schenk et al. 2018). But the physical mechanisms are not well understood yet. Thus, to estimate lifetimes, to propose methods of maintenance through oil impregnation or to better impregnate wood logs with aqueous liquid for peeling, it is necessary to continue the research efforts for improving the understanding of the mechanisms of liquid transport in relation with the structure of wood.

Wood is composed of tubular cells, with different void (i.e. lumen) sizes and arrangements (essentially tracheids for softwoods and vessels and fibers for hardwoods), eventually connected by pits on the side faces, and with characteristics depending on the localization within the growth ring (latewood or earlywood) in the case of wood from temperate regions. Moisture Content (MC) depends on the sorption mechanisms and water uptake (Almeida et al. 2007, Kekkonen et al. 2014) and is defined as the ratio of water mass to dry wood mass. Water in cell walls is named bound water and when cell walls are saturated with bound water, MC is called the Fiber Saturation Point (FSP). Water present in cell lumens is identified as free water. Considering oil imbibition tests, only lumens are filled with oil.

For most porous materials, liquid transport is basically described by the Darcy's law, which indicates that the pressure gradient is equal to the flow rate times the fluid viscosity divided by the medium permeability and the imbibition mechanism follows the Washburn law (Washburn 1921). This model predicts that the total liquid uptake is proportional to the square root of time and that a uniform liquid front advances linearly with the square root of time. In wood, either in softwoods or in hardwoods, these characteristics have been observed, for example for the front of penetration (Kučerová 2012) or for the proportionality between the total liquid uptake and the square root of time (Sedighi-Gilani 2014). However, even if some deviations from the Washburn law are observed, capillary effects are usually considered.

In Zhou et al. 2018 and 2019, for oils of different viscosities, the Washburn model is effectively in agreement with the dynamics of the process using the parameters (permeability, contact angle, pore size) of the system as deduced from direct measurements for poplar heartwood. However, this is not the case for water: spontaneous water imbibition is several orders of magnitude slower than expected from the Washburn prediction using the effective parameters of the system. In particular, observations with Magnetic Resonance Imaging (MRI) showed that bound water progresses faster than free water and that the dynamics of imbibition in poplar heartwood is partly governed by bound water progression, and then not by capillary effects.

Actually, for the comprehension of the physical mechanisms of liquid imbibition into wood, the critical point is to be able to measure its spatial distribution in time, taking into account its state. For this purpose, ^{1}H Nuclear Magnetic Resonance (NMR) is a helpful technique. In the special case of water, it allows to discriminate free and bound waters through the spin-lattice (T_1) and spin-spin (T_2) relaxation times (Zhou et al. 2018, van Meel et al. 2011, Gezici-Koç et al. 2017 and 2018, Bonnet et al. 2017, Rostom et al. 2019). Although T_1 can provide an insight in the two types of bound water (Bonnet et al. 2017), T_2 is best suited to discriminate bound water –regarded as a whole- and free water. Bound water, through the hydroxyl groups of wood

components to form the hydrogen bonds, has a short T_2-value. Free water behaves as bulk water confined in a submillimeter pore and usually exhibits a longer T_2-value (Gezici-Koç et al. 2017 and 2018), all the more long than the cell diameter is large. In some previous studies, NMR was used to distinguish and quantify bound water and free water contents by T_2 measurements (Telkki et al. 2013, Menon et al. 1987, Labbé et al. 2002). As based on the T_2-value, the dynamic of bound and free water imbibition profiles, through MRI technique, along poplar wood sample as a function of time were identified during water uptake (Zhou et al. 2018), and also the moisture profiles of water states in yellow poplar under drying condition (Zhang et al. 2013).

In this paper, we focus on the imbibition mechanisms, i.e. how aqueous liquid tends to spontaneously penetrate into softwoods in contact with it. Through an original approach coupling quantitative information obtained from mass and deformation measurements, NMR relaxation measurements and MRI observations, we are able to quantify bound and free water dynamics. To discuss these results, standard imbibition tests by weighing are also performed with water and oil and are analyzed through Washburn model.

Materials and Methods

Wood materials

Wood samples are collected from Douglas-fir (*Pseudotsuga menziesii*) planks, which had been left drying naturally under ambient conditions. Studied samples come either from the outer part of the trunk (sapwood) or from the inner part (heartwood). The average density of all specimens measured at 44% Relative Humidity (RH) is 590 (±40) $kg.m^{-3}$ for heartwood and 620 (±030) $kg.m^{-3}$ for sapwood and the proportion of latewood related to the annual ring width is estimated as 45±5% for all studied samples subjected to imbibition tests. These values are consistent with literature (Lachenbruch et al. 2010, Osborne et al. 2016) for Douglas-fir with a high proportion of latewood or for this RH. For instance, in Lachenbruch et al. 2010, the density at 12% MC is 783 $kg.m^{-3}$ with a latewood proportion of 56%.

Density essentially finds its origin in different proportions of latewood and earlywood while the general qualitative features of the material remain the same. The microstructural properties explain the physical origin of liquid transfers. Heartwood and sapwood materials are mainly composed of tracheids and a small percentage of rays is observed. The tracheids exhibit smaller diameter in latewood compared to earlywood, with a ratio between them of about 2. The average cell diameters are as follows: (heartwood) 39.4 ±4.2 µm in earlywood and 21.4 ±5.2 µm in latewood, and (sapwood) 44.7 ±4.7 µm in earlywood and 20.9 ±4.8 µm in latewood. These measured lumen diameters are consistent with those given in (Ramage et al. 2017, Vahey et al. 2007) for Douglas-fir. The cell length (along the L-axis) is approximately equal to a few millimeters and the tubular tracheids are closed at their tips but connected to each other via bordered pits on their lateral sides. The pits are located regularly along the tracheid cells. Most of bordered pits of adjacent tracheid cells in heartwood are closed in the earlywood and opened in the latewood, whereas in sapwood they are opened both in the early and latewood (Almeida et al. 2008, Sedighi-Gilani et al. 2014). Through a quantitative analysis with Douglas-fir, it has been shown in (Elaieb 2014) that about 65% of pits are open in sapwood but only 23% in heartwood. Note that the rays contain a smaller number of pits in the crossing-field which are connected to the tracheid cells. They may provide a path for internal flow, but since they are perpendicular to the main flow direction of the present study, we assume that their role is here negligible as considered in (Wardrop et al. 1961).

Wood samples and liquid

Two kinds of samples have been used: on the one hand, small cubes sawn along the anisotropic directions, R, T and L (1x1x1 cm^3 or 2x2x2 cm^3), for NMR relaxation measurements and

characterization of the wood properties and, on the other hand, for the liquid imbibition tests, large samples with about 10 cm in longitudinal (L) direction, parallel to the imbibition axis, and about 4cm and 2cm in the tangential (T) and radial (R) direction respectively, with several visible growth rings. Tests have been duplicated to check the reproducibility of the results. Samples are all pre-conditioned in desiccators at 20°C and at 44% Relative Humidity (RH) before testing. Note that for liquid imbibition tests, four of six sides of large samples are sealed with a water impermeable coating along the vertical sides parallel to the imbibition direction in order to avoid capillary effects between the external wood surface and the water bath, or possible water uptake from the lateral sides (Zhou et al. 2018). In this work, imbibition tests are performed with (deionized) water and three oils whose density, viscosity and surface tension at 25°C are respectively: Water (1000 $kg.m^{-3}$, 0.001 Pa.s, 0.073 N m^{-1}), Dodecane (740 $kg.mm^{-3}$, 0.00134Pa.s, 0.025 N m^{-1}), silicone oil 47V20 (950 $kg.m^{-3}$, 0.02 Pa.s, 0.0206 N m^{-1}) and silicone oil 47V350 (970 $kg.m^{-3}$, 0.35 Pa.s, 0.021 N m^{-1}).

As water and dodecane have close viscosities, the differences in dynamics of imbibition, if any, find their origin in differences in wood-liquid interactions or in penetration mechanisms. To compare these two liquids, small cubes are prepared and conditioned at two RH levels with saturated salt solutions (44%RH: Potassium carbonate, K_2CO_3 and 97%RH: potassium sulphate, K_2SO_4) or immersed in water or docedane oil for 3 days. MC of wood is given in Table 1. The values are obtained by drying all specimens at 103°C, in an oven, until reaching a constant mass. For samples immersed in water or oil for 3 days, the accessible porosity Φ is the volume of total water or oil to sample volume (at 44%RH) ratio. These results show that the values seem to be quite similar for heartwood and sapwood. However, these results are related to the scale of the used samples and the sample preparation by sawing may slightly increase the accessibility of fluid inside wood by opening some tracheids (Choong et al. 1975). Moreover, swelling coefficients are measured for samples subjected to RH (Table 2). These swelling coefficients are in accordance with literature (MacLean 1958, Jamaaoui 2017). Concerning dodecane oil, no swelling is observed.

NMR Relaxation measurements

For NMR measurement, small sample is inserted in a 18-mm diameter glass tube in which the humidity level is imposed (same value as for sample preparation) during the NMR relaxation experiment. This glass tube is then inserted into a Bruker Minispec MQ20 spectrometer at 0.5 T, corresponding to a resonance frequency of 20 MHz for ^1H. The T_2 relaxation measurements of the wood sample are performed using a Carr–Purcell–Meiboom–Gill (CPMG) NMR sequence by carrying out 10000 echoes with an echo time of 0.5ms. A repetition time of 12 seconds was used (much higher than 5 times T_1 in order to prevent sample heating), 8 averages were used. The NMR data are post-treated by means of an Inverse Laplace Transform (ILT) algorithm, which converts relaxation signal into a continuous distribution of T_2 values. For more details on the used homemade computer program and the artifacts of this technique, see (Faure et al. 2008).

Free water and oil distribution from MRI

Large wood samples are immersed in liquid to a depth of about 5 mm. In case of oil, the wood sample is placed in a glass Petri dish and MRI profiles are determined continuously. For water, the imbibition test is performed outside the MRI apparatus and MRI measurements are carried out at different times. The sample is put on a plastic sample support whose vertical position can be adjusted in order to be placed inside the MRI system. Measurements are performed at a vertical MRI spectrometer (DBX 24/80 Bruker) operating at 0.5 *T* and equipped with a ^1H birdcage radio frequency coil of 20 cm inner diameter, with the sample located at the magnetic

center of the gradient coil (a BGA26 Bruker, 26 cm inner diameter, 50mT/m gradient strength). As NMR relaxation times depend on the magnetic field strength, they are in principle the same in NMR relaxation and MRI experiments since both equipments have the same magnetic field.

The water or oil 1D profiles along the sample axis (Supplementary Material, Figure 1.1) are measured by means of a spin-echo sequence, with an imaging gradient in the vertical direction, and repeating the profiling process over 16 successive echoes created by a series of π pulses separated by a fixed echo-time TE=3.47ms, and selected by means of 32-step duplex cogwheel phase cycling scheme (Levitt et al. 2002). One measurement then provided a series of 16 profiles recorded at successive times TE, 2TE,…, 16TE during the spin-spin relaxation process, with a field of view of 16 cm and a space resolution of 1.25 mm. A repetition time of 7 seconds was used and 32 averages were measured. Signal intensity was calibrated using a glass tube of known diameter filled with water or oil (using a repetition time of 12 seconds and 128 averages). In the case of water, due to the short relaxation time of bound water regarding TE, only free water is detected. A monoexponential or biexponential fit was then used to quantify the amount of liquid inside wood taking into account the relaxation times T_2 (see below).

The 2D distribution (image) of free water or oil was observed by means of multi-slice 2D MRI during the imbibition test. 2D MRI vertical slices of 2 mm thickness with 2-mm interval between them (parallel to RL plane) passing through the wood sample with space resolution equal to 0.47 (radial and tangential) × 2.19 (longitudinal) mm are taken at different times during imbibition (Supplementary Material, Figure 1.1). A multi-slice multi-echo (MSME) pulse sequence acquiring 8 echoes was used with an echo time of 10 ms and a recycle delay of 600 ms. On purpose of enhancing the signal to noise ratio without increasing the measurement time, images intensities owing the each of the 8 echoes were added to produce the final picture. This picture can only be used for the qualitative purpose of seeing where the fluid is. Note that in the case of water, this weighing enhances the signal intensity of water in the large lumens of the earlywood due to longer T_2 time, which will be of key importance for data interpretation.

Bound water distribution from swelling measurements

To identify and quantify bound water distribution along the wood samples during water imbibition tests with large samples, it is proposed to use swelling measurements after some preliminary analysis providing the relation between the deformation to the bound water content for small samples subjected to RH as done by (Zhou et al. 2018). The sample swelling is measured along the radial (R) and tangential (T) directions every 5 mm along the longitudinal direction (L) using a micrometer (Mitutoyo) with a precision of 0.01 mm for large samples subjected to imbibition tests. For each distance, two different locations along the longitudinal direction are considered to obtain an average value for both directions R and T.

Figure 1 shows the linearity of the relation observed between the bound water mass and the corresponding sample volume increase on small samples. This result allows to determine a "coefficient" of bound water mass per unit volume increase, which we will use later on to translate the sample deformation during imbibition tests in bound water. Furthermore, the calculated swelling coefficients (Table 2) show that the variation of the volume may be only evaluated from the measurements of the dimensions along the radial and tangential directions, as the swelling coefficient is negligible along the longitudinal direction. As no swelling is observed during oil imbibition tests, this further supports the idea that strains are strictly related to bound water during water imbibition, and this means that MRI profiles for oil imbibition will in principle show the full amount of oil impregnating the sample. The total water mass entering the samples measured by weighing is compared to the bound water mass evaluated from volume variations plus the free water mass in wood determined from integration of the MRI 1D profiles (Figure 2). It appears that the total water content entering the sample during imbibition test is

very close to the amount of bound water and free water inside wood. This confirms a very good accuracy in quantifying the total free water in wood from 1D MRI method as well as in computing bound water amount from deformation measurements.

Standard imbibition tests by weighing

A bottom open surface of the sample is placed (along a height of about 5 mm) in contact with a bath of liquid (water or oil) covered by a film to avoid evaporation (Supplementary Material, Figure 1.2). Liquid can then progress inside wood along its longitudinal direction. The other open surface is connected to a precision balance via a hanging wire. The mass evolution of the sample is recorded by a precision balance through an automatic recording system. The imbibition test is carried out at room temperature (20°C). Note that the apparent mass has to be corrected to get the effective mass due to a buoyancy force varying with the liquid level in the bath (Supplementary Material, section 1).

A quantitative analysis of the imbibition tests may be done through the Washburn model as explained below (for more details, see Zhou et al. 2018 and 2019). At the front of penetration inside the sample (interface), the average capillary ascent of a liquid in a porous material (with cylindrical conduit of radius R) is driven by the capillary pressure (neglecting ambient pressure): $\Delta p=-2\sigma cos\theta/\alpha R$, where σ is the surface tension, α a factor related to the pore shape and θ the contact angle. This driving force acts over a distance of penetration h, which induces a pressure gradient p/h. The Darcy's law then expresses the balance between the pressure gradient and the viscous resistance with $\Delta p/h=\mu V/k$ where μ is the liquid viscosity, V the mean flow velocity through the sample, and k the permeability of the porous medium. Assuming that the liquid advances as a front saturating the lumens below a distance $h=\Omega/\varepsilon S$ increasing in time (where Ω is the volume of water entered in the sample and S the section of the sample), $V=(d\Omega/dt)/S=\varepsilon(dh/dt)$, with ε the (accessible) medium porosity. Integrating the Darcy's law we deduce that in a first regime controlled by capillary effects (negligible gravity effects) we have:

$$\varepsilon h = \Omega/S = \lambda\sqrt{t/\mu} \quad (1)$$

with $\lambda=\sqrt{2k\varepsilon\sigma\cos\theta/\alpha R}$, which is independent of the liquid viscosity.

In a second regime controlled by gravity effects, h tends to a plateau h_{max} determined by:

$$h \to h_{\max} = \frac{\sigma\cos\theta}{\alpha R\rho g} \text{ when } t \to \infty \quad (2)$$

Then, since the main geometrical characteristics of the hydraulic system are known, the fundamental unknown of the problem is the contact angle, which may be fitted to either the dynamics or the maximum height of ascent. Note that if the porosity ε is not taken into account in the previous relationships, this amounts to just consider an "apparent" height for the progression of liquid.

For the flow through a cylindrical capillary, we have $\alpha = 1/2$ (the meniscus is a spherical cap) and the velocity profile can be computed exactly (Poiseuille law), which directly gives the relation between the pressure gradient and the mean velocity, from which we deduce the permeability for a set of parallel capillaries:

$$k = \varepsilon R^2/8 \quad (3)$$

Results and discussion

NMR Relaxation times for dodecane and water

Figure 3 presents the distribution of NMR intensity as a function of T_2 for heartwood and sapwood at 44%RH and 97%RH and after 3 days of immersion in water or dodecane.

In the case of immersion in water, three main peaks are observed for heartwood and sapwood. The first peak with a T_2 value surrounding 1 ms corresponds to the bound water at

44%RH and 97%RH and after 3 days of immersion in water (Gezici-Koç et al. 2017). This peak is located at the very limit of T_2 times that can be measured with the CPMG sequence, and is just a -non quantitative - clue of a - true - fast relaxing peak of bound water existing for T_2<1ms. When the bound water content increases, the true peak increases in intensity and is shifted to higher T_2 due to the increased mobility of water molecules in cell walls (Bonnet et al. 2017), thus leading to an increase and a small shift of the apparent peak which can be clearly observed. Two other wide peaks are identified for both heartwood and sapwood. As admitted in literature (Almeida et al 2007 and Gezici-Koç et al. 2017), these peaks are attributed to free water. They are located at roughly 10 and 50 ms for heartwood and 17 and 70 ms for sapwood. These two peaks depend on the lumen sizes, and the longer T_2 is attributed to earlywood (Kekkonen et al. 2014, Menon et al. 1987). Note that, for heartwood, the two peaks are well-separated, but not for sapwood. Variability in pore sizes maybe simply related to uncertainty in the ILT processing but also to the seasonal variability of the wood structure. For sapwood, the T_2 distribution may reflect the polydispersity of the pore sizes (Gezici-Koç et al. 2017) and the presence of a transition zone between earlywood and latewood.

In the case of dodecane immersion, essentially one peak is obtained, situated at relatively large T_2-values (about 955 ms and 992 ms for heartwood and sapwood respectively). Here the surface relaxivity (i.e. the proportionality constant between T_2 decay time and pore size) is very small so that the influence of pore size on the T_2 relaxation time of dodecane is weak (Zhou et al. 2018). Also, a small peak at low relaxation time is visible in each case, which likely corresponds to bound water as the sample is pre-conditioning at 44%RH.

Distribution of dodecane and free water from MRI and of bound water from swelling measurements

Figure 4 shows MRI 2D images of dodecane and water entering in heartwood and sapwood samples at different times. Furthermore, the 1D curve profiles (Figure 5) provide a quantification of their penetration into samples as a function of time. In the case of water imbibition, as explained previously, only free water is observed with MRI, and bound water profiles are obtained from swelling measurements.

In the case of dodecane imbibition for heartwood (Figure 4a) its penetration in earlywood is very limited (up to about 3-5 mm) and dodecane content seems to increase in this layer with time. Above 5 mm, dodecane seems to preferentially penetrate in latewood along the vertical axis of the sample up to the top of the sample. However, it remains that the MRI signal for the 2D images is very weak (same order of magnitude as the signal-to-noise ratio), and effectively the 1D profiles show a very limited amount of dodecane entering into the sample (Figure 5a). As the relaxation time is the same in early- and latewood, then a monoexponential fit is used to quantify the total amount of oil and it is not possible to distinguish in both latewood and earlywood. In the case of sapwood, the 2D images clearly show that some dodecane reaches the top of the sample after only 3 hours of imbibition test, in agreement with the 1D profiles with higher content of dodecane oil (Figure 4b and Figure 5b). Moreover, dodecane seems to preferentially penetrate in the earlywood, but there may be some penetration in latewood, not well visible on these images. The differences of dodedane penetration into heartwood or sapwood may be explained by the fact that there are more open pits in sapwood, as explained in the section “Wood materials”.

These results also show that for both types of wood, dodecane apparently does not progress in the form of a uniform (straight) front saturating the sample at larger heights in time, as expected from the standard Washburn imbibition process. However, dodecane imbibition profiles showing a liquid profile extending widely throughout the material but of level increasing in time, suggest that the material imbibition proceeds by a progressive increase of

the local saturation throughout the material. This aspect of the liquid profile results from the heterogeneity of the material, while in each tracheid the liquid progresses as a straight front: the dynamics of climbing varies from one tracheid to another, so that along some axis the liquid may have already reached the sample top while in another place the liquid is much less advanced. Such a heterogeneous distribution of front advances can predict this profile aspect.

According to the 2D images for free water (Figures 4c and 4d), the water front is climbing in a jagged manner and clearly corresponds to the location of earlywood and latewood layers. The heartwood provides an extremely slow water uptake which seems limited to a height of about 5 mm after 6 days, with a progression front slightly higher in latewood. For sapwood, a higher water uptake is observed with a water front reaching up to 35-40 mm over the same duration. However, as explained previously, two T_2 relaxation times for free water are observed due to the presence of different lumen sizes. By this means we can now distinguish the distribution of free water in each type of wood in time using a bi-exponential fit (Figures 5c and 5d). It appears that in sapwood the free water advances over significant distance in both wood types (earlywood and latewood); in contrast, in heartwood, the free water seems to hardly be able to reach a height larger than a few millimeters. These observations are consistent with the qualitative observations from 2D MRI images.

Furthermore, according to the profiles of bound water, the most important result is that the bound water distribution extends farther than the profile of free water, an effect particularly clear for heartwood. So it can be considered that bound water at least partly propagates by itself longitudinally through the cell walls. In particular, bound water uptake seems to be quite constant up to the front of penetration of free water, with a moisture content close to the FSP (taking into account the moisture content at 44%HR, Table 1). This suggests that basic characteristics of water transport in softwood qualitatively similar to that in hardwoods (Zhou et al. 2018), i.e. a dynamics of imbibition mainly governed by the longitudinal progression of bound water in the sample: free water can advance through the vessels (considered as opened capillary tubes with unlimited length) only when cell walls are saturated with bound water. However, in the case of softwood, the mechanisms for liquid water transport may be quite different as the structure is different with tracheids, with limited length, closed at their ends and connected to each other by pits.

To conclude, in coherence with Sedighi-Gilani et al. 2012 and 2014, the water uptake is significantly larger for sapwood than for heartwood. This result is similar for oil penetration. The liquid transport penetration in heartwood and sapwood may depend on open or closed pits. Furthermore, for both materials, larger oil and water contents are localized in the first 5 mm, due to possible effect of preparation of sample. Indeed, sawing may slightly increase the accessibility of fluid inside wood by opening tracheids (Choong et al. 1975). The aim of the next section is to precise the involved mechanisms for both materials, through Washburn model and from the standard imbibition tests.

Discussion through standard imbibition tests by weighing

Imbibition results for water and oil are expressed in terms of the liquid volume entering into wood, per sample area (expressed as “apparent height”) as a function of the time rescaled by the liquid viscosity (Figure 6). This representation is useful to discuss the imbibition dynamics of different liquids with regards to the Washburn model (Equation (1)). The data deduced from MRI experiments are also shown in the same graph and an excellent agreement is found between these data and those obtained from mass measurements. In Supplementary Material (section 2), the volume of water or oil per sample area as a function of time and 2D MR images for the three oils at the end of the imbibition tests are also shown for further discussions. Note that for a cylindrical capillary containing, from place to place perturbations (e.g. pits) of its

shape over very short distance, the maximum height of ascent is that of the main cylinder, since the liquid must be able to climb between two successive perturbations, and thus Equation (2) is still valid with R the main cylinder radius. Furthermore, the permeability may be affected (decreased) by these perturbations as they induce further viscous dissipation during the liquid flow through the whole system. It follows that the dynamics may be damped with regards to that expected for the flow through a simple straight conduit but the Washburn law remains valid.

Concerning sapwood (Figure 6a), the curves for oils of different viscosities (with only slight differences in surface tension and likely close contact angles) superimpose along a master curve when the time is rescaled by the viscosity. This demonstrates the validity of the assumption of a viscous flow through a given hydraulic network at the origin of liquid uptake (for example in consistency with the form of Equation (1)). In contrast, the imbibition curve for water, with a surface tension different from that of oil by a factor about 3, is situated at rescaled times about 100 larger than the master curve for oils. The point may be more directly appreciated from the representation of water uptake as a function of time (Supplementary Material, section 2): dodecane and water have a similar viscosity but a surface tension different by a factor 3, but the water uptake is slower by several orders of magnitude than that of oil. This means that in that case the flow is not dependent on the same physical effects underlying the Washburn approach for imbibition. This result is discussed in the following trough Washburn model. A plateau in the imbibition curve is clearly observed for Dodecane around Ω/S=1.3 cm (Figure 6a, Equation (2)). Considering the accessible porosity of sapwood determined on small samples (Table 1) for oil (i.e. 29.7%), this corresponds to an effective average maximum height of ascent around $h_{max} = (\Omega/\varepsilon S) = 4.4$ cm. This may be in agreement with the 2D MRI images of Dodecane oil, which show liquid signal at larger height, if we assume that the tracheid diameters are somewhat dispersed around a mean value, allowing different final heights of ascent around this one, up to the sample height (i.e. 10 cm). It is also possible that the accessible porosity, determined from oil impregnation in small samples, was somewhat overestimated due to tracheid opening when sawing, as explained previously. Finally, note that the results for oils of different viscosities are consistent with the 2D MRI images providing the qualitative aspect of liquid ascent (Supplementary Material, section 2). From Equation (2), using R = 15µm for the average radius of tracheids (without distinguishing latewood and earlywood), a contact angle of $\Theta \approx 84°$ is calculated. Then, from the slope λ of the imbibition curve (Equation 1), the permeability value of the Washburn model may be deduced, i.e. $k = 0.35 \times 10^{-12}$ m^2. It is worth noting that this value is of the same order as the permeability of a set of simple capillaries with the same mean radius (Equation (3)), i.e. $k = \varepsilon R^2/8 = 8.4 \times 10^{-12}$ m^2, which confirms assumption of oil flow through tracheids. The smaller permeability value obtained here would then likely be explained by the existence of pits and direction changes all along the hydraulic network leading to additional pressure drops. Finally, this tends to confirm that in sapwood the hydraulic network is made of tracheids connected by open pits. As explained above, the oil imbibition process maybe due to the heterogeneity of the tracheid sizes, which leads to a distribution of Washburn imbibition with different characteristic times. It might alternatively be due to an imbibition process involving the fast ascent of some fluid towards large heights coupled with a more progressive imbibition in smaller pores at the different heights. To sum up: Washburn model is valid along each series of connected tracheids, which explain that the observed dynamics is consistent with the theoretical prediction, associated with a front step propagation in this series, but the different dynamics in each of them may give the impression of a partial saturation at different levels.

For water imbibition in sapwood, we observe a maximum apparent height (Ω/S) of ascent similar to that found for oils, which leads to a similar value for the contact angle. Since from

such tests, as water (bound or free) cannot be distinguished, the total accessible porosity of the system for water is considered (about 41.9%, Table 1), to compute the maximum height of ascent, which resumes to considering that both phases approximately fill their own porosity at the same rate. The predicted front of penetration (Equation 2) is then: $h_{max}= (\Omega/\varepsilon S)$=3.0 cm. This value is in agreement with the (average) front of propagation determined with MRI 1D profiles for both free and bound water, for about 3 days of imbibition tests (Figure 5d). A contact angle of $\Theta \approx 88°$ is then obtained, which is the hallmark of a poor wetting. Then, from the slope λ of the imbibition curve, we deduce the permeability value of the Washburn model, i.e. $k = 3 \times 10^{-15}$ m^2. This permeability is several orders of magnitude lower than that expected for a set of simple capillaries with the same mean radius (Equation 3), i.e. $k = \varepsilon R^2/8 = 11.8 \times 10^{-12}$ m^2. It is also several orders of magnitude smaller than the permeability observed with oil, which cannot solely be explained by the difference of accessible porosity to water. It is worth noting that, although there is some significant uncertainty on the effective maximum height of ascent in the tracheids, this does not affect this conclusion, i.e. using a different value for the accessible porosity during the process would still lead to this very large discrepancy between the apparent permeability and that associated with a standard Washburn ascent along the tracheids.

Imbibition results for heartwood strongly differ from those in sapwood (Figure 6b). First of all, the maximum height reached is significantly lower (about three times) than that in sapwood over similar duration, both for oil and water. Another remarkable point is that the curves for the different oils or water do not superimpose when the time is rescaled by the viscosity. These results may not be explained by the variability of samples (for instance the density due to different proportions of latewood as mentioned above). In fact, the shift between them approximately correspond to the viscosity factor, which means that the curves would roughly superimpose if represented as a function of time (without rescaling by the viscosity). And effectively, when the volume of oil per sample area entering into sample is represented as a function of the (non-rescaled) time the curves superimpose (Supplementary Material, Figure 2.1). This implies that in that case the uptake of oil is independent of viscous effects, and thus cannot be described by the standard Washburn approach which relies on a balance between capillary and viscous effects. The estimation of the permeability gives value of the same order as that observed for water in sapwood. Altogether these different observations confirm that here the pits are preferentially closed, so that there is only negligible flow through the hydraulic system up to the top of the sample. Concerning water, as for sapwood, from MRI measurements, the bound water profile progresses in advance of free water, but in this case, the dynamics of free water imbibition seems not to be mainly governed by the longitudinal progression of bound water in the sample. Then only a small amount of water can penetrate in the structure, essentially by diffusion through cell walls. However, it is not clear how it can occur for oil, considering that oil essentially penetrates in the first 5mm, the amount above 5mm being significantly lower due to closed pits. The preferentially penetration in the first 5mm layer may be explained by the existence of open tracheids following cutting during the sample preparation. Above a few millimeters, liquid hardly progress in the tracheids because of preferentially closed pits and with their limited length.

Discussion on the mechanisms of free water imbibition

All these results obviously mean that the propagation of water does not rely on the basic physical assumptions underlying the Washburn model. Instead we have to consider that the capillary transport may be damped by some effect. Since the pits are moist sensitive it may be suggested that pits could tend to close when in contact with water while letting oil move through. However, in that case we would expect some similar dynamics between heartwood (for which pits are preferentially closed) and sapwood. This is not what we observe (Figure 6b):

the dynamics of water imbibition is apparently about six times faster in sapwood than in heartwood. Moreover, in the case of heartwood, there is almost no free water penetrating the sample within the duration of the test (Figure 5c), as a result of closed pits, whereas a significant amount of free water apparently penetrates the sapwood region, meaning that in contrast pits effectively remain open in sapwood (Figure 5d).

Actually, it is worth noting that bound water progresses through the sample more rapidly than free water in heartwood and sapwood (Figures 5c and 5d) and water uptake seems to be governed by bound water diffusion and not by capillary flow as expected by the Washburn law. This is similar to an effect suggested for aspen heartwood by (Johansson et al. 2011) but not for aspen sapwood. This result is still not fully understood. However, as explained above, the climbing of free water is allowed only when the free water is in contact with cell-walls which MC is close to the FSP, otherwise there is a negligible displacement of free water; under such conditions the dynamics is governed by the coupling between the longitudinal diffusion of bound water and the progressive advance of free water.

According to Zhou et al. 2019, this is associated with a strong change of the wetting properties with the concentration of bound water: X-Ray synchrotron images indeed showed that the apparent contact angle during imbibition was close to 90° while it was seen to be much lower when the cell walls are saturated with bound water, which explains the need of sufficient longitudinal diffusion of bound water before the water can further progress through the lumens. Finally, note that these results seem to be supported by the MRI observations of Dvinskikh et al (Eng. Structures, 2011) and Eiltelberg et al (2011) for a spruce sample simply put in contact with air at a large RH. In that case, even in the absence of free water in contact with the sample, bound water was observed to rapidly propagate in the longitudinal direction, showing its ability to diffuse relatively rapidly thus keeping the possibility to control the liquid transport in an imbibition process.

Conclusion

The aim of this study was to analyze the mechanisms of liquid transport in Douglas-fir, especially in heartwood and in sapwood. To answer to this question, two kinds of tests have been performed to identify the mechanisms of water and oil penetration: NMR methods and standard imbibition tests by weighing.

Concerning the oil penetration, our results show that the Washburn law is only verified for sapwood. In the case of heartwood, our results show that the uptake of oil is independent of viscous effects, and thus cannot be described by the standard Washburn approach which relies on a balance between capillary and viscous effects.

For the case of water, the phenomena are more complex, as it is necessary to take into account free water and bound water, and the Washburn law is not available for sapwood and heartwood. Indeed, our results show that the front penetration of liquid water is mainly governed by the longitudinal progression of bound water in the sample.

Acknowledgements

This work has benefited from a French government grant managed by ANR within the frame of the national program Investments for the Future ANR-11-LABX-022-01 (Labex MMCD, http://mmcd.univ-paris-est.fr/).

References

Almeida, G., Gagne, S., Hernandez, R.E. (2007) A NMR study of water distribution in hardwoods at several equilibrium moisture contents, Wood Science and Technology, 41:293–307.

522 Almeida, G., Leclerc, S., Perre, P. (2008) NMR imaging of fluid pathways during drainage of
523 softwood in a pressure membrane chamber, International Journal of Multiphase Flow,
524 34:312–321.

525 Bao, F., Siau, J.F., Avramidis, S. (1986) Permeability and capillary structure of Chinese woods.
526 Wood and Fiber Science, 18(2): 220–227.

527 Bonnet, M., Courtier-Murias, D., Faure, P., Rodts, S., Care, S. (2017) NMR determination of
528 sorption isotherms in earlywood and latewood of Douglas fir. Identification of bound water
529 components related to their local environment, Holzforschung, 71(6):481–490.

530 Choong, E.T., McMillin, C.W., Tesoro, F.O. (1975) Effect of surface preparation on gas
531 permeability of wood, Wood Science, 7(4):319-322.

532 Dupleix, A., Denaud, L., Bleron, L., Marchal R., Hugues M. (2013) The effect of log heating
533 temperature on the peeling process and veneer quality: beech, birch, and spruce case studies.
534 Eur. J. Wood Prod. 71:163–171.

535 Dvinskikha S.V, Henrikssonb M., Mendicino A.L., Fortino, S., Toratti, T. (2011) NMR
536 imaging study and multi-Fickian numerical simulation of moisture transfer in Norway
537 spruce samples, Engineering Structures 33(11):3079-3086.

538 Elaieb, M.T. (2014) Amélioration de l'imprégnabilité aux solutions aqueuses des duramens des
539 résineux : Le cas du Douglas (Pseudotsuga Menziesii Franco), Thèse de l'Université de
540 Lorraine. In French.

541 Elaieb, M.T., Petrissans, A., Elkhorchani, A., Marchal, R., Pétrissans, M. (2016) Influence of
542 drying on douglas-fir heartwood impregnability to water, Innovation in woodworking
543 industry and Enginerring design, 1(9): 54–62.

544 Eitelberger J., Hofstetter K., Dvinskikh S.V. (2011) A multi-scale approach for simulation of
545 transient moisture transport processes in wood below the fiber saturation point, Composites
546 Science and Technology, 71(15):1727-1738.

547 Faure P., Rodts S. (2008) Proton NMR relaxation as a probe for setting cement pastes. Magn
548 Resonance Imaging 26:1183–1196.

549 Gezici-Koç, O., Erich, S.J.F., Huinink, H.P., van der Ven, L.G.J., Adan, O.C.G. (2017) Bound
550 and free water distribution in wood during water uptake and drying as measured by 1D
551 magnetic resonance imaging, Cellulose, 24:535–553.

552 Gezici-Koç, O., Erich, S.J.F., Huinink, H.P., van der Ven, L.G.J., Adan, O.C.G. (2018)
553 Understanding the influence of wood as a substrate on the permeability of coatings by NMR
554 imaging and wet-cup, Progress in Organic Coatings, 114:135–144.

555 Jamaaoui A., (2017) Durabilité et comportement hygroscopique du Douglas en relation avec
556 son patrimoine génétique, Thèse de doctorat de génie civil de l'Université de Limoges. In
557 French

558 Johansson, J., Salin, J.G. (2011) Application of percolation modelling on end-grain water
559 absorption in aspen (Populus tremula L.), Wood Material Science and Engineering,
560 6(3):112–118.

561 Kekkonen, P.M., Ylisassi, A., Telkki, V.V. (2014) Absorption of water in thermally modified
562 pine wood as studied by nuclear magnetic resonance, Journal of Physical Chemistry C,
563 118(4): 2146–2153.

564 Kučerová I., (2012) Methods to measure the penetration of consolidant solutions into 'dry'
565 wood, Journal of Cultural Heritage, 13(3): S191-S195.

566 Labbé, N., De Jéso, B., Lartigue, J.-C., Daudé, G., Pétraud, M., Ratier, M. (2002) Moisture
567 content and extractive materials in maritime pine wood by low field 1H NMR,
568 Holzforschung 56:25–31.

569 Lachenbruch, B., Johnson, G.R., Downes, G.M., Evans, R. (2010) Relationships of density,
570 microfibril angle, and sound velocity with stiffness and strength in mature wood of Douglas-
571 fir, Canadian Journal of Forest Research, 40(1):55–64.

572 Levitt, M., Maduh, P., Hughes, C. (2002) Cogwheel phase cycling, Journal of Magnetic
573 Resonance, 155:300–306.

574 MacLean, J.D. (1958) Effect of moisture changes on the shrinking, swelling, specific gravity,
575 air or void space, weight and similar properties of wood, Madison, Wis. : U.S. Dept. of
576 Agriculture, Forest Service, Forest Products Laboratory.

577 van Meel, P.A., Erich, S.J.F., Huinink, H.P., Kopinga, K., Jong, J.D., Adan, O.C.G. (2011)
578 Moisture transport in coated wood, Progress in Organic Coatings 72:686– 694.

579 Menon, R.S., MacKay, A.L., Hailey, J.R.T., Bloom, M., Burgess, A.E., Swanson, J.S. (1987)
580 An NMR determination of the physiological water distribution in wood during drying,
581 Journal of Applied Polymer Science, 33:1141–1155.

582 Osborne, N.L., Høibø, Ø.A., Maguire, D.A. (2016) Estimating the density of coast Douglas-fir
583 wood samples at different moisture contents using medical X-ray computed tomography
584 Computers and Electronics in Agriculture, 127:50–55.

585 Ramage, H.M., Burridge, H., Busse-Wicher, M., Fereday, G., Reynolds, T., Shah, D.U., Wu,
586 G., Yu, L., Fleming, P., Densley-Tingley, D., Allwood, J., Dupree, P., Linden, P.F.,
587 Scherman, O. (2017) The wood from the trees: The use of timber in construction, Renewable
588 and Sustainable Energy Reviews, 68:333–359.

589 Rostom, L., Courtier-Murias, D., Rodts, S., Caré, S. (2019) Investigation of the effect of aging
590 on wood hygroscopicity by 2D ^{1}H NMR relaxometry, Horlzforshung, online.

591 Sedighi-Gilani, M., Griffa, M., Mannes, D., Lehmann, E., Carmeliet J., Derome, D. (2012)
592 Visualization and quantification of liquid water transport in softwood by means of neutron
593 radiography, International Journal of Heat and Mass Transfer, 55:6211–6221.

594 Sedighi-Gilani, M., Vontobel, P., Lehmann, E., Carmeliet, J., Derome, D. (2014) Liquid uptake
595 in Scots pine sapwood and hardwood visualized and quantified by neutron radiography,
596 Materials and Structures, 47:1083–1096.

597 Schenk, H.J, Espino, S., Rich-Cavazos, S.M., Jansen S. (2018) From the sap's perspective: The
598 nature of vessel surfaces in angiosperm xylem, American Journal of Botany 105(2): 1–14.
599 Siau, J.F. (1995) Wood: Influence of moisture on physical properties. Dept. of Wood Sci.
600 and Forest Prod., Virginia Tech, Blacksburg, VA. 227 pp

601 Telkki, V.V., Yliniemi, M., Jokisaari, J. (2013) Moisture in Softwoods: Fiber Saturation Point,
602 Hydroxyl Site Content, and the Amount of Micropores as Determined from NMR Relaxation
603 Time Distributions, Holzforschung, 67: 291–300.

604 Vahey**,** D.W., Zhu, J. Y., Scott, C.T. (2007) Wood density and anatomical properties in
605 suppressed-growth trees : comparison of two methods, Wood and fiber science. 39(3):462-
606 471.

607 Zhang, M, Wang, X., Gazo, R. (2013) Water states in yellow poplar during drying studied by
608 time domain nuclear magnetic resonance, Wood and Fiber Science, 45(4):423–428.

609 Zhou, M., Caré, S., Courtier-Murias, D., Faure, P., Rodts, S., Coussot, P. (2018) Magnetic
610 resonance imaging evidences of the impact of water sorption on hardwood capillary
611 imbibition dynamics, Wood Science and Technology, 52(4):929–955.

612 Zhou, M., Caré, S., King, A., Courtier-Murias, D., Rodts, S., Gerber, G., Aimedieu, P., Bonnet,
613 M., Bornert, M., Coussot, P. (2019) Liquid uptake governed by water adsorption in
614 hygroscopic plant-like materials, Physical Review Research, 1:033190

615 Wardrop, A.B., Davies, G.W. (1961) Morphological factors relating to the penetration of
616 liquids into woods, Holzforschung, 15(5):129-141.

617 Washburn, E.W. (1921) The dynamics of capillary flow, Physical Review, 17:273–283

618

619

620 **TABLES**

621

622 **Table 1**: Moisture Content MC (%) and accessible porosity Φ (%). Mean and Standard
623 Deviation (SD) values are given (three samples).

	MC at 44% RH	MC at 97% RH	MC (3 days in water)	Φ (3 days in water)	Φ (3 days in oil)
Sapwood	10.2 (±0.1)	25.3 (±0.35)	79.4 (±3.7)	41.9 (±1.2)	29.7 (±0.1)
Heartwood	10.5 (±0.1)	20.5 (±0.25)	75 (±0.15)	39.1 (±3.2)	23.9 (±2.0)

624

625 **Table 2**: Swelling coefficients α (%/%) along the anisotropic directions R, T, L. Mean and
626 Standard Deviation (SD) values are given (three samples).

	α (R)	α (T)	α (L)
Sapwood	0.17 (±0.02)	0.40 (±0.01)	0.007 (±0.004)
Heartwood	0.14 (±0.02)	0.20 (±0.003)	0.02 (±0.01)

627

628

FIGURES

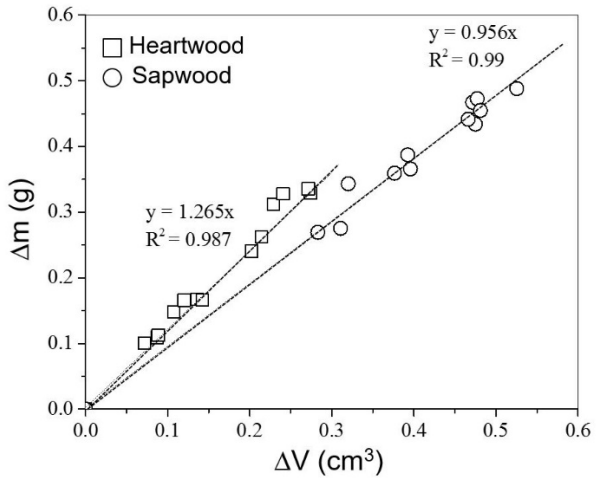

Figure 1: Additional mass Δm of bound water recorded by weighing as a function of volume increase ΔV (determined on small samples) for heartwood and sapwood between 44% RH to 97% RH.

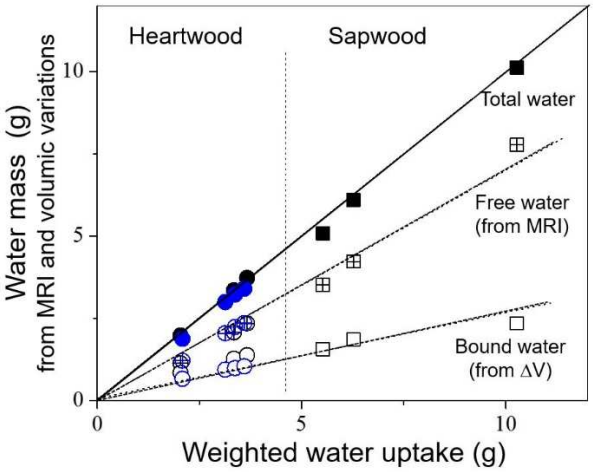

Figure 2: Free water mass (from MRI) plus bound water (from swelling measurements ΔV) compared to the total water uptake determined by weighing, at different times during imbibition tests with large samples for heartwood (black or blue circle symbols for two tests) or for sapwood (black square symbols).

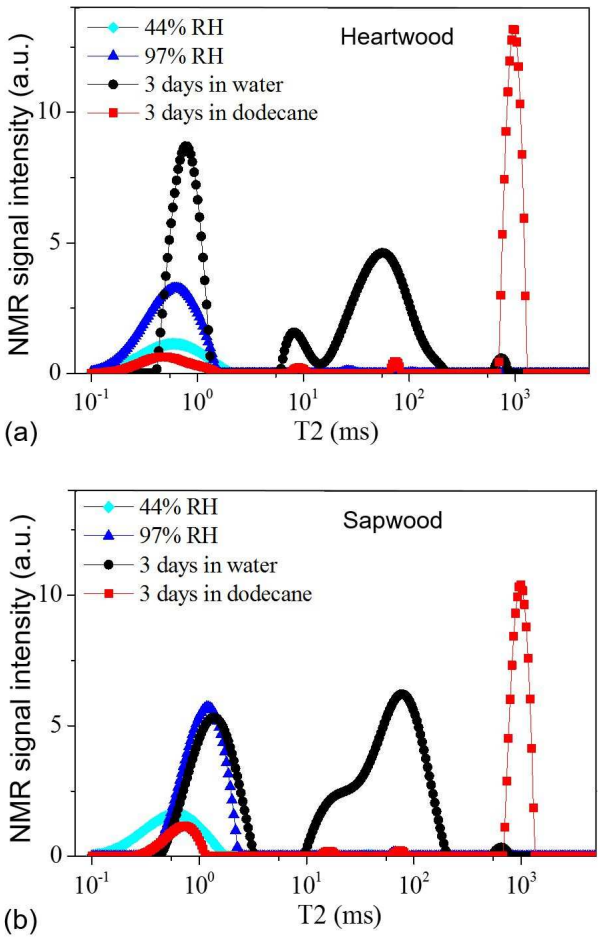

Figure 3: NMR T_2 relaxation times for heartwood (a) and sapwood (b) under 44% or 97% RH and after 3 days of immersion in water or dodecane.

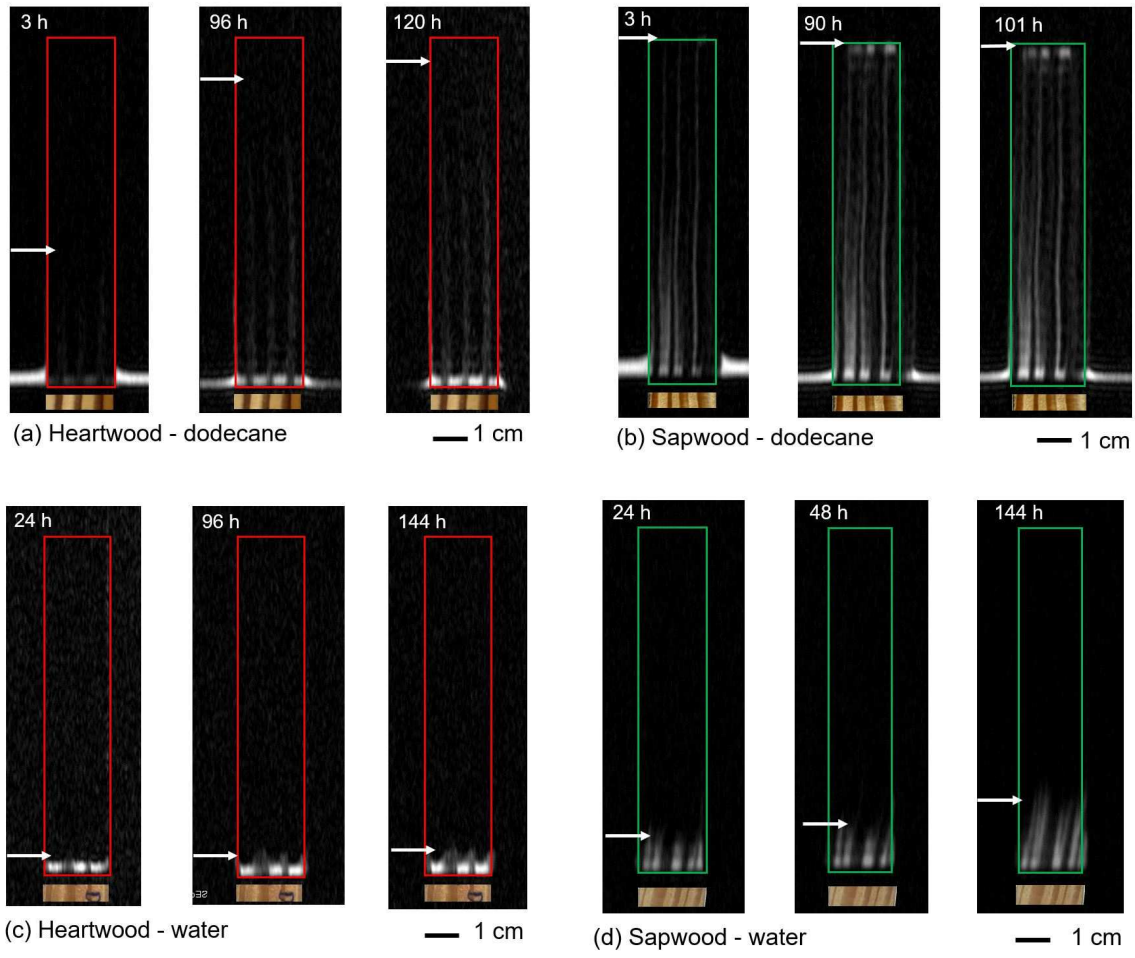

Figure 4: 2D MRI images (longitudinal-radial plane) of dodecane oil and free water distribution in wood samples at different times during imbibition tests for heartwood (a, c) and (b, d) for sapwood. The front of liquid penetration is indicated by a white arrow according to the 1D profiles given in Figure 5. A view of the sample cross section is inserted showing the correspondence between the main liquid paths and the sample structure (latewood and earlywood).

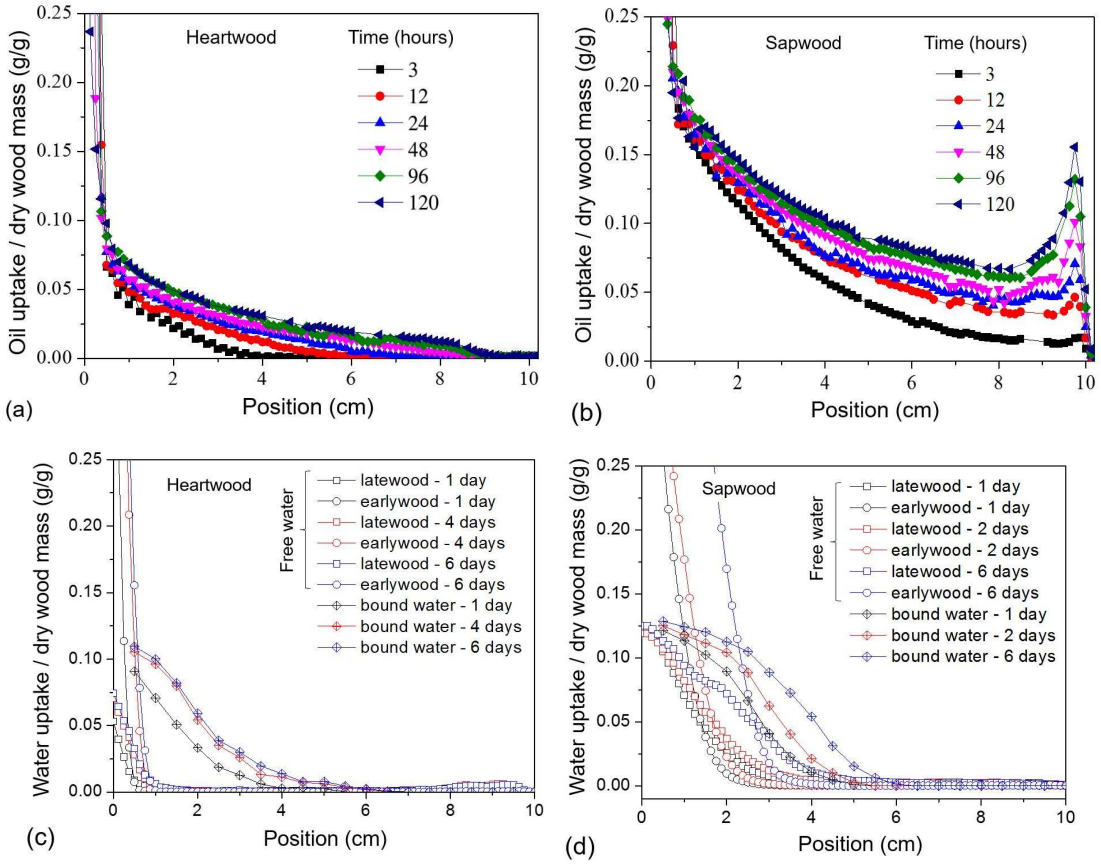

Figure 5: 1D MRI profiles of oil (dodecane) and water uptake at different times for heartwood (a, c) and sapwood (b, d).

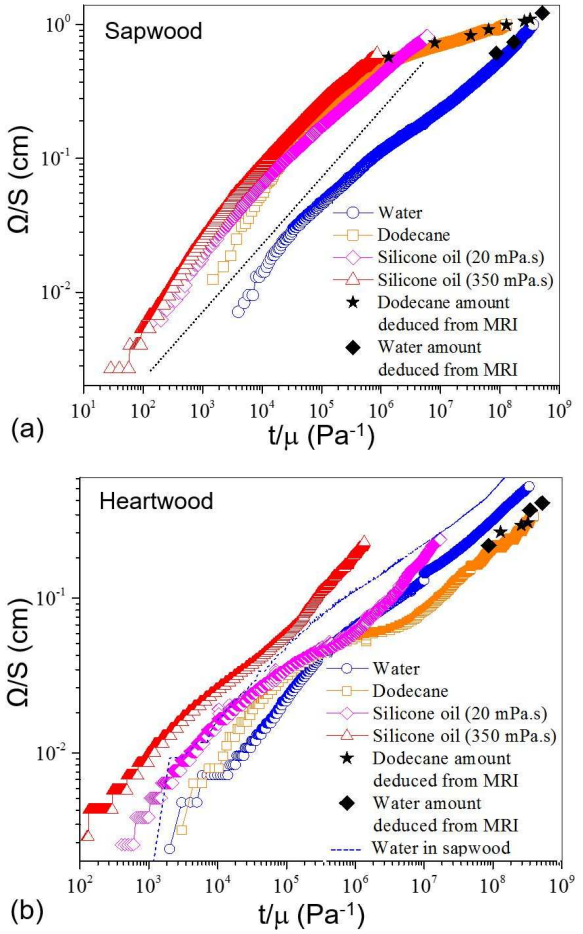

Figure 6: Absorbed liquid volume per unit cross-section Ω/S area against the time per viscosity t/μ of water, dodecane oil and two silicone oils for sapwood (a) and heartwood (b) samples. The dashed line of slope 2 in Fig. a is a guide for the eye.

SUPPLEMENTARY MATERIAL

Mechanisms of liquid imbibition in Douglas-fir inferred from ^{1}H Nuclear Magnetic Resonance methods

Dang Mao NGUYEN [1], Sabine CARE [1, *], Denis COURTIER-MURIAS [1], Meng ZHOU [1], Philippe COUSSOT [1]

[1] *Lab. Navier, Ecole des Ponts, Univ Gustave Eiffel, CNRS, Marne-la-Vallée, France*

* sabine.care@univ-eiffel.fr

SECTION 1: IMBIBITION TESTS

Principles of MRI measurements and of standard imbibition tests by weighing

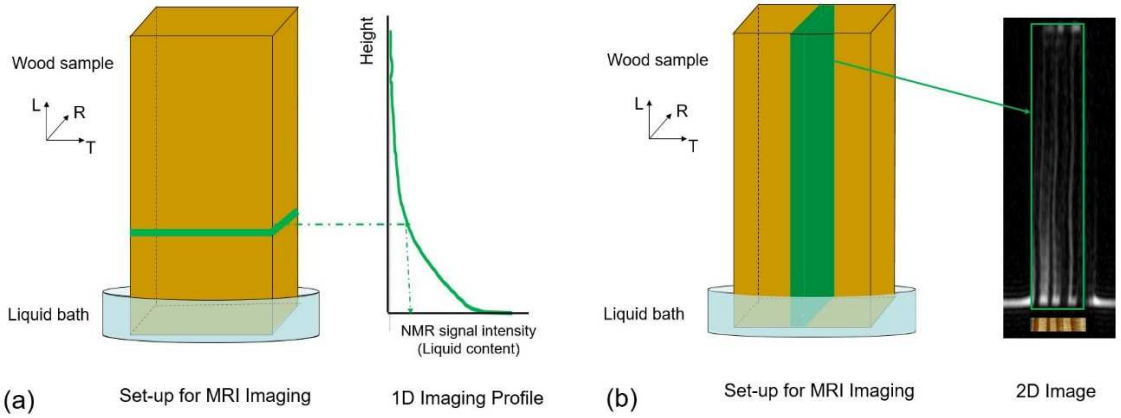

Figure 1.1: Principle of the imbibition experiments, showing the orientation of the wood sample, whose vertical faces have been sealed with paint and of the different MRI measurements (for more details, see Zhou et al. 2018, 2019): a) Projection of transverse signal for 1D profiles along sample axis. Every point corresponds to the integrated signal in the horizontal slice with 1.25 mm of thickness. b) Slice selection for 2D NMR imaging. Examples are given for dodecane oil imbibition.

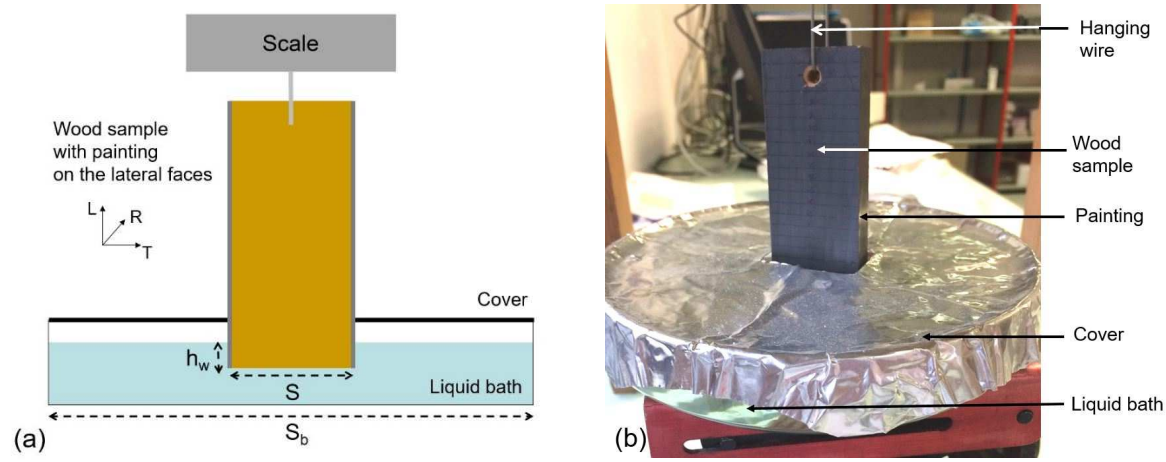

Figure 1.2: Scheme of the standard imbibition test by weighing. a) Principle of the measurements. b) View of the experiments. See below for the definitions of S_b, S and h_w.

Correction of buoyancy force

The variation of buoyancy force referred to the initial state can been written as $-\rho S\Delta h_w$, with ρ the liquid density, S the cross-section area of the wood sample and $\Delta h_w$the variation of wetted height.

The apparent mass of liquid entered in the sample thus writes

$$m_0 = m - \rho S\Delta h_w \quad \text{(S.1)}$$

where m is the effective entered mass.

Futhermore, the variation of liquid level in the bath results from this mass entrance:

$$m = \rho(S_b - S)\Delta h_w \quad \text{(S.2)}$$

where S_b is the cross-section area of the liquid bath.

Using the value for Δh_w deduced from equation (S.1), in the expression (S.2) we find the expression for the effective entered mass of liquid:

$$m = m_0(1 - S/S_b) \quad \text{(S.3)}$$

SECTION 2: RESULTS

Liquid volume per sample area against time

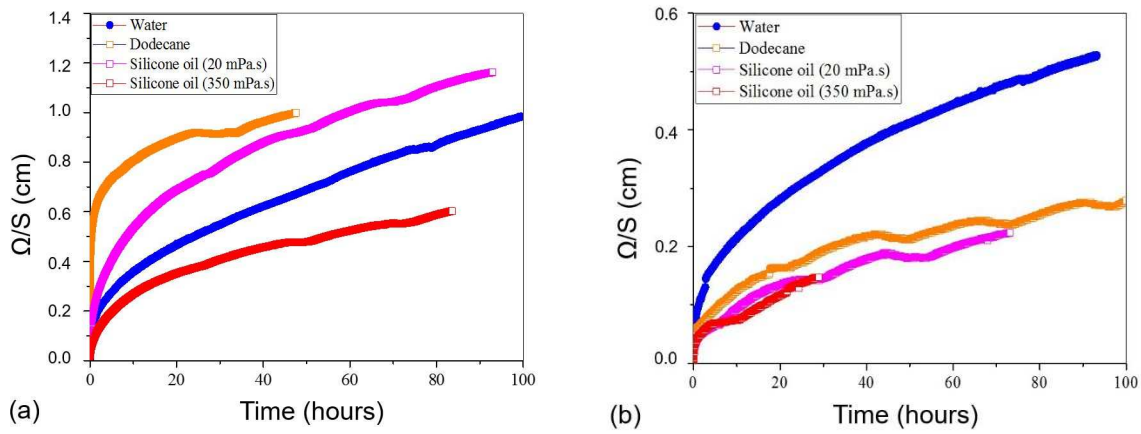

Figure 2.1: Liquid (oils and water) volume per sample area (cm) against time (hours) for sapwood (a) and heartwood (b). Initial state for all samples: 44% RH. Tests have been duplicated for heartwood to confirm these "unexpected results".

712 **MRI 2D images for the three oils (47V350, 47V20 and dodecane)**

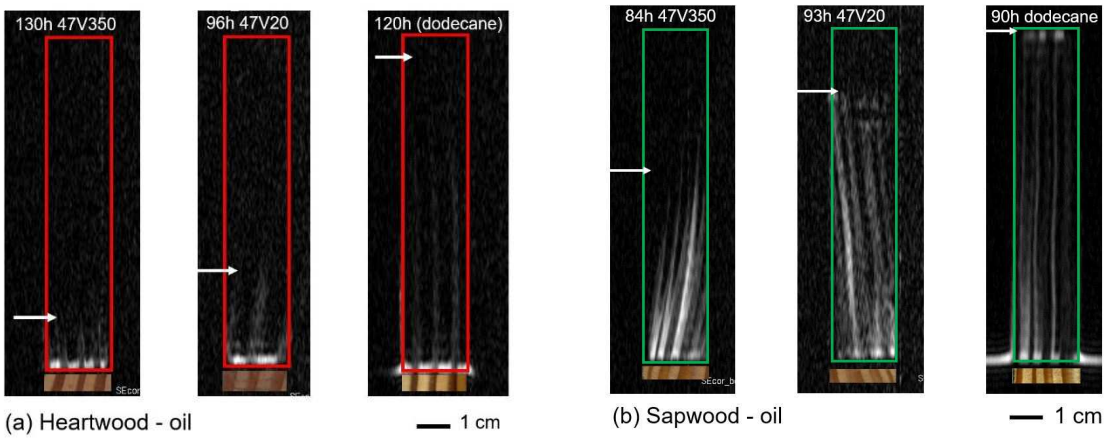

713

714 **Figure 2.2**: 2D MRI images of the oil imbibition test along the longitudinal direction at the end
715 of the test for three oils (47V350, 47V20 and dodecane). Longitudinal-radial plane images: (a)
716 for heartwood and (b) for sapwood. A view of the sample cross section is inserted showing the
717 correspondence between the main oil paths and the sample structure (presence of latewood
718 or earlywood). The front of oil penetration is indicated by a white arrow.

719 ## REFERENCES

720 Zhou, M., Caré, S., Courtier-Murias, D., Faure, P., Rodts, S., Coussot, P. (2018) Magnetic
721 resonance imaging evidences of the impact of water sorption on hardwood capillary imbibition
722 dynamics, Wood Science and Technology, 52(4):929–955.

723 Zhou, M., Caré, S., King, A., Courtier-Murias, D., Rodts, S., Gerber, G., Aimedieu, P., Bonnet,
724 M., Bornert, M., Coussot, P. (2019) Liquid uptake governed by water adsorption in hygroscopic
725 plant-like materials, Physical Review Research, 1:033190

726